International Journal of Heat and Mass Transfer 181 (2021) 121996

Contents lists available at ScienceDirect

International Journal of Heat and Mass Transfer

journal homepage: www.elsevier.com/locate/hmt

Thermophoresis and its effect on particle impaction on a cylinder for low and moderate Reynolds numbers

Nils Erland L. Haugen[a,b,*], Jonas Krüger[a], Jørgen R. Aarnes[c], Ewa Karchniwy[c,d], Adam Klimanek[d]

[a] SINTEF Energy Research, Trondheim N-7465, Norway
[b] Nordita, KTH Royal Institute of Technology and Stockholm University, Roslagstullsbacken 23, Stockholm SE-10691, Sweden
[c] Department of Energy and Process Engineering, Norwegian University of Science and Technology, Kolbjørn Hejes vei 1B, Trondheim NO-7491, Norway
[d] Institute of Thermal Technology, Silesian University of Technology, Konarskiego 22, Gliwice 44-100, Poland

ARTICLE INFO

Article history:
Received 11 March 2021
Revised 14 September 2021
Accepted 20 September 2021
Available online 30 September 2021

Keywords:
Particle deposition
Thermophoresis
Overset grids

ABSTRACT

The effect of thermophoresis on the impaction of particles on a cylinder is investigated for different particle sizes, particle conductivities, temperature gradients and for Reynolds numbers between 100 and 1600. This is the first such study performed using Direct Numerical Simulations (DNS), where all temporal and spatial scales of the fluid are resolved. Simulations are performed using the Pencil Code, a high-order finite difference code with an overset-grid method precisely simulating the flow around the cylinder.

The ratio of particles impacting the cylinder to the number of particles inserted upstream of the cylinder is used to calculate an impaction efficiency. It is found that both the particle conductivity and the temperature gradient have a close to linear influence on the particle impaction efficiency for small particles. Higher Reynolds numbers result in higher impaction efficiency for middle-sized particles, while the impaction efficiency is smaller for smaller particles. In general, it is found that thermophoresis only has an effect on the small particles, while for larger particles the impaction is dominated by inertial impaction.

An algebraic model is presented that predicts the effect of the thermophoretic force on particle impaction on a cylinder. The model is developed based on fundamental principles and validated against the DNS results, which are faithfully reproduced. As such, this model can be used to understand the mechanisms behind particle deposition due to the thermophoretic force, and, more importantly, to identify means by which the deposition rate can be reduced. This is relevant for example in order to minimise fouling on super-heater tube bundles in thermal power plants.

1. Introduction

Particle impaction on surfaces can be found in a multitude of industrial systems, such as filters and heat exchangers. The impaction and deposition of material on these surfaces can significantly alter their performance, necessitating decreased maintenance intervals or an increased rate of replacement of components. In order to improve the design of surfaces exposed to particle laden flows, a thorough understanding of the underlying effects is needed.

In this work, we will focus on how particles are transported to the solid surface. For a particle to deposit on the surface, it must first be transported to the surface, before it has to stick to it. The latter mechanism is outside the scope of this study. In the following, all particles impacting on the surface will therefore be counted towards particle deposition.

The transport of material to the surface is governed by the impaction efficiency. The impaction efficiency is defined as the ratio of particles that actually come in contact with the cylinder to particles that would come in contact with the cylinder if they were unaffected by the change in fluid velocity due to the presence of the cylinder. For an overview of the progress and challenges in the field of particle impaction in coal and biomass-fired systems, the reader is referred to the review of Kleinhans et al. [1].

Due to its simplicity, a cylinder placed in a particle laden flow is a widespread test case used to study the impaction of particles on solid surfaces or heat exchanger tubes. A sketch of such a case is shown in Fig. 1, where the particles (shown in green) are inserted from a plane (red) that has the same size as the projected area

* Corresponding author at: SINTEF Energy Research, N-7465 Trondheim, Norway.
E-mail address: nils.e.haugen@sintef.no (N.E.L. Haugen).

https://doi.org/10.1016/j.ijheatmasstransfer.2021.121996

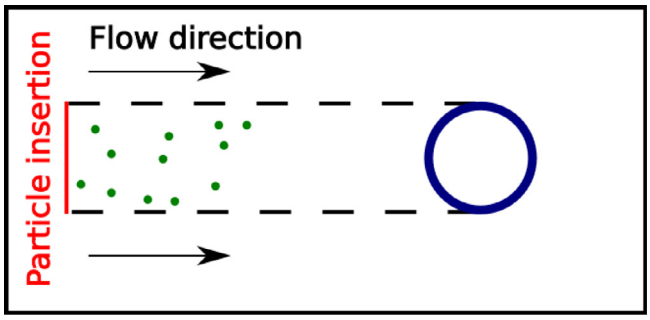

Fig. 1. Sketch of particle deposition analysis case.

of the cylinder. The initial velocity of the particles is equal to the flow velocity at the insertion plane. If the particles followed the flow from left to right, without any change in velocity, all particles would hit the cylinder, leading to an impaction efficiency (η) of unity. For all realistic cases $\eta < 1$, as the fluid is flowing around the cylinder and particles are dragged along with it. A particle's ability to follow the fluid is expressed as the particle's Stokes number, St, which is the ratio of the particle response time and the fluid time scale (details in Section 2.2). In general, particles with Stokes numbers above unity do not follow the flow very well, while the opposite is true for particles with small Stokes numbers.

Israel and Rosner [2] developed a correlation based on potential flow theory, which allows for calculation of impaction efficiency on an isothermal cylinder. This correlation is a well established tool for predicting the isothermal impaction efficiency of *large* particles in a laminar flow, but it is highly inaccurate for *small* particles [3], and it is undefined for Stokes numbers below 0.125.

The mass accumulation rate on a cylinder is determined by the capture efficiency – the product of the impaction efficiency and the sticking efficiency. The sticking efficiency is the fraction of the impacting particles that stick to the surface rather than rebound. If either the particles or the cylinder surface is at least partially melted, the sticking efficiency is close to unity. On the other hand, for cold and clean surfaces, particles will most likely bounce off the surface, and the sticking efficiency is close to zero.

The experimental study by Kasper et al. [4], investigated the effect of mass accumulation on the capture efficiency and proposed an empirical power law for it. Moreover, the authors presented a new fit function for the capture efficiency, which is bounded between 0 and 1. The particle Stokes numbers in said study were between 0.3 and 3. Haugen and Kragset [3] investigated the impaction efficiency using Direct Numerical Simulation with an immersed boundary method and found a steep drop in impaction efficiency below a certain Stokes number, as particles become smaller and follow the flow better. Extending this work, Aarnes et al. studied the same case using overset grids, obtaining results that are deemed more accurate with significantly less computational effort [5,6].

The effect of thermophoresis on the capture efficiency is studied by several groups, both experimentally and numerically. Beckmann et al. [7] measured deposition of fly ash from a pulverised coal jet flame and simulated the deposition rate using Reynolds Averaged Navier Stokes (RANS) based CFD with the $k-\epsilon$ model. They found that thermophoresis increases the capture efficiency for smaller particles, and that the relative increase is higher the smaller the particles in question are. Experimental data from a pilot-scale furnace was compared to numerical results by Yang et al. [8], where the influence of deposition growth on the particle impaction and sticking efficiency was studied. In this work, the RANS approach of Ansys Fluent was used for the numerical simulations. They reported that the higher surface temperature due to deposit growth results in a reduced effect of thermophoresis and an increased sticking efficiency. At later times, the rate of shedding of material from the surface and deposition of material on the surface from the flow balance out, so no net change of the mass of the deposit is observed [9].

In the work of Kleinhans et al. [10] the effect of the thermophoretic force was studied both experimentally and numerically. In the experimental part, the deposition of material on cooled and un-cooled probes that are inserted into the particle laden flow above the burner section of a combined heat and power (CHP) plant was studied. Large-Eddy simulations (LES) were used to study the influence of the sticking model and thermophoresis on deposition rate predictions. The authors present a model that can take into account different sticking mechanisms by which large and small particles of different composition deposit. It was reported that thermophoresis accounts for three quarters of the observed deposition rate. García Prez et al. [11] used unsteady RANS simulations to study the effect of thermophoresis on particle deposition and found that the thermophoretic force was the dominating deposition mechanism for very small particles.

The effect that the thermophoretic force has on particle impaction on a cylinder in a cross-flow is controlled entirely by processes occurring in the boundary layer around the cylinder. As such, it is essential that the boundary layer is completely resolved in order for simulations of the process to have any predictive abilities. RANS simulations, and to some extent LES, involve crude approximations and cannot guarantee that the high accuracy required to properly resolve the boundary flow is achieved to such extent that trajectories of small particles affected by thermophoretic forces are accurately computed. Direct Numerical Simulations (DNS) is a highly time-consuming method for flow simulations, where all spatial and temporal scales are resolved, applicable for cases where very high accuracy is paramount.

To the knowledge of the current authors, DNS have not previously been used to perform a parameter study of the effect of the thermophoretic force on the particle deposition rate on a cylinder in a cross flow. This motivates the authors of the current study to investigate the influence of different flow conditions, such as flow Reynolds number, temperature gradient and particle attributes on the effect of thermophoresis. Furthermore, no generic analytical model describing the effect that the thermophoretic force has on particle impaction on a cylinder in a cross flow exist. Such a model will be developed in the following section. The model will later be validated against the DNS results. The novelty of the current study is therefore twofold: 1) the first ever accurate DNS of particle impaction under a wide range of conditions and 2) an analytical model, based on fundamental principles, that predicts and explains the effect that the thermophoretic force has on the impaction rate.

2. Theory

2.1. Fluid equations

The governing fluid equations are the compressible equations for continuity, momentum and energy. Pressure is taken into account through the ideal gas law and the Mach number is ≈ 0.1, low enough to consider the flow as essentially incompressible. The continuity equation is given by

$$\frac{\partial \rho}{\partial t} + \boldsymbol{u} \cdot \nabla \rho = -\rho \nabla \cdot \boldsymbol{u}, \tag{1}$$

with ρ, t and $\boldsymbol{u}$ being density, time and velocity, respectively. The equation governing the conservation of momentum is

$$\rho \frac{\partial \boldsymbol{u}}{\partial t} + \rho \boldsymbol{u} \cdot \nabla \boldsymbol{u} = -\nabla p + \nabla \cdot (2\rho \nu S), \tag{2}$$

where p is the pressure, ν the kinematic viscosity, and

$$S = \frac{1}{2}\left(\nabla \boldsymbol{u} + (\nabla \boldsymbol{u})^T\right) - \frac{1}{3} I \nabla \cdot \boldsymbol{u} \tag{3}$$

is the rate of strain tensor where I is the identity matrix. The energy equation is solved for temperature by

$$\frac{\partial T}{\partial t} + \boldsymbol{u} \cdot \nabla T = \frac{k_f}{\rho c_v} \nabla^2 T + \frac{2\nu S^2}{c_v} - (\gamma - 1) T \nabla \cdot \boldsymbol{u}, \tag{4}$$

where $\gamma = c_p/c_v = 5/3$, c_v and c_p are the heat capacities at constant volume and pressure, respectively, and k_f is the thermal conductivity. The ideal gas law is used to tie pressure and density together:

$$p = \rho r_u T, \tag{5}$$

where $r_u = c_p - c_v$ is the specific gas constant. To simplify the investigation, the kinematic viscosity, ν, is assumed to be constant since the temperature variations in the fluid are relatively small. In this study, the Pencil Code is used to solve the governing equations. Since the code is an explicit compressible DNS code, the time step, dt, is limited by the speed of sound through the CFL number, i.e., $dt = C_{CFL} \times \min(\Delta_{\text{mesh}})/(c_s + \max(u))$, where Δ_{mesh} is the mesh spacing, $C_{CFL} = 0.8$ is the CFL number, and the speed of sound is given by $c_s = \sqrt{\gamma r_u T} = \sqrt{c_p(\gamma - 1)T}$. One can therefore use c_p as a free parameter in order to artificially lower the speed of sound to obtain larger time steps. This is a valid approach as long as the Mach number is kept lower than 0.1 and the viscous heating of the fluid is negligible. To maintain a constant thermal diffusivity ($D_{\text{thermal}} = k_f/(\rho c_p)$) of the gas phase, and hence a constant Prandtl number ($\text{Pr} = \nu/D_{\text{thermal}}$), the conductivity ($k_f$) is changed proportionally to the specific heat capacity of the fluid (c_p).

2.2. Particle equations

The particles considered here are spherical and have low Biot numbers, making them spatially isothermal. Numerically they are treated as point particles that are influenced by the fluid, but are too dilute to have any significant back-reaction on the fluid. In other words, they are acted on by the flow but have no effect on it. This assumption is applicable for dilute flows, which is the focus of the current work. The particle size is described by its Stokes number

$$\text{St} = \frac{\tau_{\text{St}}}{\tau_f}, \tag{6}$$

where $\tau_{\text{St}} = \frac{S_\rho d_p^2}{18\nu}$ is the particle Stokes time and $\tau_f = \frac{D}{u}$ is the flow time scale. Here, $S_\rho = \frac{\rho_p}{\rho}$ is the density ratio between particle and fluid, d_p is the particle diameter and D is the diameter of the cylinder. Two forces are acting on the particle: the drag force and the thermophoretic force (gravity is neglected for the small particles studied here). The drag force is given by:

$$\boldsymbol{F}_D = \frac{m_p}{\tau_p}(\boldsymbol{u} - \boldsymbol{v}_p), \tag{7}$$

where τ_p, m_p and $\boldsymbol{v}_p$ are the particle's response time, mass and velocity, respectively. Using the Stokes time with the Schiller-Naumann correction term [12] to account for low to moderate particle Reynolds numbers, yields the particle response time

$$\tau_p = \frac{\tau_{\text{St}}}{f}, \tag{8}$$

where

$$f = 1 + 0.15\text{Re}_p^{0.687} \tag{9}$$

and $\text{Re}_p = d_p|\boldsymbol{v}_p - \boldsymbol{u}|/\nu$ is the particle Reynolds number.

The thermophoretic force pushes particles from regions of high temperature to regions of low temperature. As such, it is similar to the Soret effect for gases. It was first observed in 1870 by Tyndall [13], and it has later become widely studied both experimentally and theoretically. A theoretical analysis of the thermophoretic force can be found in the works of Zheng [14]. Young [15] gives an overview over the different regimes of thermophoresis, which are determined by the particles Knudsen number $\text{Kn} = \lambda/d_p$, where λ is the mean free path of the gas. For the present study, all particles are in the continuum regime ($\text{Kn} \ll 1$), hence the thermophoretic force is calculated by

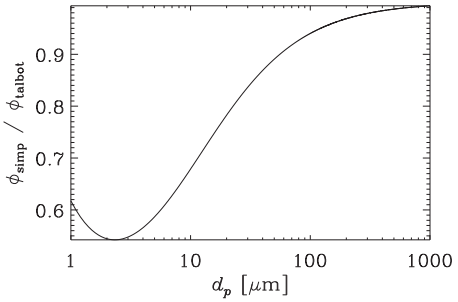

Fig. 2. Comparison of different thermophoretic force terms.

$$\boldsymbol{F}_{th} = \Phi \frac{\mu^2 r_p \nabla T}{\rho T}, \tag{10}$$

where $r_p = d_p/2$ is particle radius, $\mu = \rho\nu$ is dynamic viscosity and Φ is the thermophoretic force term. The expression for Φ is taken from Epstein [16]:

$$\Phi = \frac{-12\pi K_{tc}}{2 + \Lambda}, \tag{11}$$

where the conductivity ratio between the particle and the gas is given by $\Lambda = k_p/k_f$, while the temperature creep coefficient, K_{tc}, used in this work has a value of 1.1, which is in the middle of the range reported by Sharipov [17]. This rather simple model for Φ simplifies the analysis, while still providing agreeable results when compared with the widely used approach proposed by Talbot et al. [18]. From Fig. 2 we see that the largest relative difference between the simplified Φ and the one obtained when using the approach of Talbot is less than a factor of two.

2.3. Theory

Due to their short response times, very small particles will follow the fluid almost perfectly, essentially behaving like tracer particles. For isothermal situations, Haugen and Kragset [3] showed that a small fraction of these particles will nevertheless impact on the cylinder surface due to their small but finite radii.

For the non-isothermal case, where the temperature of the cylinder is lower than that of the surrounding gas, the thermophoretic force will induce a relative velocity between the particles and the fluid that transport the particles in the direction towards the cylinder. The effect of this is that a larger fraction of the particles impact on the cylinder surface. In the following we will try to quantify this effect.

For laminar flows, a fluid streamline that starts far upstream of the cylinder with a displacement Δx from the central line (the line parallel to the mean flow, going through the centre of the cylinder) will move in the boundary layer of the cylinder with a radial displacement from the cylinder surface of $\Delta r_f \neq \Delta x$ (see Fig. 3). Far upstream of the cylinder, the mass flow rate between a streamline and the center line of the cylinder is given by

$$\dot{m}_u = H u_0 \rho_0 \Delta x, \tag{12}$$

where Δx is the distance between the streamline and the centre line and H is the height of the cylinder. Within the boundary layer

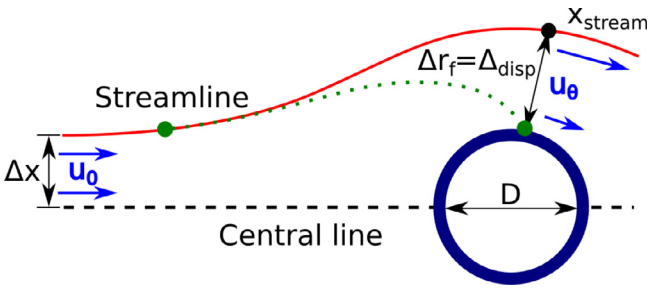

Fig. 3. Sketch of a particle track of a particle with a small Stokes number under the influence of thermophoresis.

of the cylinder, however, the mass flow rate between the streamline and the cylinder surface is given by

$$\dot{m}_b = \int_0^{\Delta r_f} \rho H u_\theta dr_{\text{cyl}} = \frac{\overline{\rho} H u_0 \text{Re}^{1/2}}{2BD} (\Delta r_f)^2, \tag{13}$$

where $\overline{\rho}$ is the average fluid density within the boundary layer. By following Haugen and Kragset [3], we have used the fact that the tangential fluid velocity within the boundary layer is given by

$$u_\theta(r_{\text{cyl}}) = \frac{u_0 \text{Re}^{1/2}}{BD} r_{\text{cyl}}, \tag{14}$$

where u_0 is the far field fluid velocity, B is a constant of the order of unity and r_{cyl} is the normal distance from the cylinder surface.

The impaction efficiency for a stationary non-turbulent flow is given by

$$\eta = 2\Delta x_{\text{max}}/D, \tag{15}$$

where Δx_{max} is the maximum Δx inside which the particles can start out in order to impact on the surface. Since streamlines of laminar flows do not cross each other, it is clear that for a given type of particles, all particles inside Δx_{max} will impact on the cylinder surface while none of the particles outside of Δx_{max} will impact. From now on, a particle starting out at the limiting distance of Δx_{max} away from the centre-line will be referred to as the last impacting particle. For Reynolds numbers above ≈ 48, the flow will become unsteady and von Krmn eddies will occur in the wake of the cylinder. The effect of this unsteadiness on the front side impaction is minor. Back side impaction may, however, be strongly affected by the von Krmn eddies. Since the focus of the current work is to study front side impaction, the definition of the impaction efficiency as given by Eq. (15) will also be used for unsteady flows.

The above equations can be solved to find the impaction efficiency for small particles by calculating the distance, Δ_{disp}, a particle will move in the radial direction due to the thermophoretic force during the time it is in the front side boundary layer of the cylinder, and setting this distance equal to Δr_f. In the following, the focus will therefore be on finding Δ_{disp}. Here, small particles are defined as particles that are so small that the main cause of impaction is the thermophoretic force. This is typically the case for $\text{St} \lesssim 0.1$.

By combining Eq. (7) and Eq. (10), while setting the radial component of the gas phase velocity to zero, we find the thermophoretic velocity of the particles (in the radial direction) as

$$v_{\text{th}} = \frac{\Phi \nu}{6\pi f} \frac{\nabla T}{T}. \tag{16}$$

The correction term to the Stokes time, as given by f (see Eq. (9)), is always close to unity if the thermophoretic force is the main driver of the particle velocity relative to the surrounding fluid. We therefore set $f = 1$ for the remainder of this analysis. From Prandtl's concept of thin boundary layers, we know that the thickness of the velocity boundary layer can be approximated by

$$\delta_{\text{vel}} = \frac{D}{\text{Re}^{1/2} B}. \tag{17}$$

The thermal boundary layer thickness is then given by Schlichting [19]

$$\delta_{\text{thermal}} = \delta_{\text{vel}} \text{Pr}^{-1/3}. \tag{18}$$

Hence, the average thermal gradient in the boundary layer becomes

$$\nabla T \approx \frac{\Delta T}{\delta_{\text{thermal}}} = \frac{\Delta T}{D} B \text{Re}^{1/2} \text{Pr}^{1/3}. \tag{19}$$

The effect of the thermophoretic force on the position of the particle can now be considered as the radial displacement of the particle (Δ_{disp}) from the position (x_{stream}) it would have without the influence of the thermophoretic force (see Fig. 3). This radial displacement is given by

$$\Delta_{\text{disp}} = v_{\text{th}} \tau_{\text{th}}, \tag{20}$$

where

$$\tau_{\text{th}} = \frac{D}{u_\theta(\Delta_{\text{disp}})} \tag{21}$$

is the time the particle stays within the front side boundary layer and $u_\theta(\Delta_{\text{disp}})$ is the tangential velocity of the flow in the boundary layer a distance Δ_{disp} away from the surface of the cylinder (see Fig. 3). From Eqs. (14) and (21) we can now find the time that the last impacting particle stays within the cylinder boundary layer before it hits the boundary as

$$\tau_{\text{th}} = \frac{BD^2}{u_0 \text{Re}^{1/2} \Delta_{\text{disp}}}. \tag{22}$$

Combining Eq. (22) with Eq. (16), Eqs. (19) and (20), and solving for Δ_{disp}, then yields

$$\Delta_{\text{disp}}^2 = \frac{\Phi B^2 \text{Pr}^{1/3} D^2}{6\pi \text{Re}} \frac{\Delta T}{T}, \tag{23}$$

where we use that $\text{Re} = u_0 D/\nu$. Since the fluid is not turbulent (i.e., streamlines do not cross each other), we know from mass conservation that the mass flux between the streamline and the central line upstream of the cylinder ($\dot{m}_u$) is equal to the mass flux between the streamline and the cylinder surface ($\dot{m}_b$). Having found Δ_{disp} from Eq. (23), we therefore proceed by setting the two mass fluxes defined in Eqs. (12) and (13) equal to each other and solve for Δx_{max} to find

$$\Delta x_{\text{max}} = \frac{\overline{\rho}}{\rho_0} \frac{\text{Re}^{1/2}}{2BD} \Delta_{\text{disp}}^2. \tag{24}$$

In the above we have used the fact that $\Delta x = \Delta x_{\text{max}}$ when $\Delta r_f = \Delta_{\text{disp}}$. From Eq. (15), we now find that for a non-negligible temperature difference, the capture efficiency for small Stokes numbers ($\text{St} \lesssim 0.1$) is given by

$$\eta = \frac{2\Delta x_{\text{max}}}{D} = \frac{\Phi B \text{Pr}^{1/3}}{6\pi \text{Re}^{1/2}} \frac{\Delta T}{T} \frac{\overline{\rho}}{\rho_0} = \frac{2K_{tc} B \text{Pr}^{1/3}}{\text{Re}^{1/2}(2+\Lambda)} \frac{\Delta T}{T} \frac{\overline{\rho}}{\rho_0}. \tag{25}$$

For laminar flows, Haugen and Kragset [3] found that B is independent of Reynolds number but varies with angular position on the cylinder surface. In particular, they found $1/B$ to be very small at the front stagnation point while the minimum value of B was found to be 0.45 at a position 60 degrees further downstream. For the remainder of this paper we chose $B = 1.6$, which is a value that yields good model predictions. In order to obtain the last part of Eq. (25), we have used the simplified version of the thermophoretic force term (Φ), but any version can be used here.

The above approach, yielding an impaction efficiency due to thermophoretic forces for small Stokes numbers, is strictly applicable only when the distance the particle travels within the boundary layer is less than a fraction α of the thickness of the boundary layer itself, i.e. when

$$\frac{\Delta_{\text{disp}}}{\delta_{\text{thermal}}} = B^2\sqrt{\frac{2K_{tc}\,\text{Pr}\,\Delta T}{(2+\Lambda)T}} < \alpha. \tag{26}$$

We shall later see that the critical value of α is somewhere between 0.5 and 1.

3. Numerical methods

The simulations for the present work are performed using the Pencil Code, an open source, highly parallelizable code for compressible flows with a wide range of implemented methods to model different physical effects [20–22].

The effect of thermophoresis on the impaction efficiency is studied by releasing a large number of particles upstream of a cylinder in an established quasi-steady flow field. Every time step, new particles are inserted at random positions on the particle insertion plane (shown as a red line in Fig. 1) with a velocity that is equal to the inlet fluid velocity. The domain is two-dimensional and has a width of $6D$ and a length of $12D$, where D is the diameter of the cylinder. The flow enters the domain on the left and leaves the domain through the outlet on the right. Navier-Stokes characteristic boundary conditions are applied at both inlet and outlet to ensure that they are non-reflective for acoustic waves [23]. All other boundaries are periodic. A cylindrical overset grid is placed around the cylinder to accurately represent the cylinder at low computational cost. This cylindrical grid communicates with the Cartesian background grid via its outer points. Summation-by-parts is used for derivatives on the surface of the cylinder, and a Padé filter is used to mitigate high frequency oscillations on the cylindrical grid. For details concerning the cylindrical overset grid, including accuracy assessment and validation, the reader is referred to Aarnes et al. [5], 6], 24].

The background grid uses 288 and 576 cells for the width and length, respectively, except for the cases with Reynolds number of 1600, where the resolution is doubled. The cylindrical grid has 144 cells in the radial and 480 cells in the tangential direction for the cases with Reynolds numbers up to 400, and double the amount for the case with a Reynolds number of 1600. The resolution increase is done to ensure that the boundary layer - scaling as $1/\text{Re}^{1/2}$ - is accurately resolved at $\text{Re} = 1600$. Grid stretching in the radial direction of the overset grid is used to ensure approximately matching cell sizes on the outer grid points of the cylindrical cells, where the background and the overset grids communicate. The code uses a sixth-order finite difference scheme for spatial discretisation and a third-order Runge-Kutta scheme for temporal discretisation. Since the cell size close to the cylinder surface is much smaller than the general cell size of the background grid, the time step of the background grid can be a multiple of the time step of the cylindrical grid, with the cylindrical flow being updated more often. For details of the particle tracking scheme, the reader is referred to Haugen and Kragset [3] or Aarnes et al. [6].

4. Simulations

The inflow temperature is 873 K and the density is 0.4 kg/m^3, corresponding to the density of air at this temperature and a pressure of 1 bar. The particle material density is 400 kg/m^3, yielding a density ratio S_ρ of 1000 based on the fluid density under inlet conditions. These values are chosen based on their relevance for particle deposition on super-heater tubes in thermal power plants. The results are nevertheless generic since they are given as functions of non-dimensional numbers. The cylinder temperature is implemented as a Dirichlet boundary condition and set to a fixed value. The inflow velocity u_0 is set so that the flow Reynolds number $\text{Re} = u_0 D/\nu$ is 100 for the reference case. For the cases studying the Reynolds number effect, the viscosity is changed to obtain different Reynolds numbers. To study the same range of Stokes numbers, the particle size is adjusted accordingly, and the thermal diffusivity is decreased to achieve a constant Prandtl number. The different aspects of the thermophoretic effect are analysed by changing one critical parameter at the time, while holding the others constant. These critical parameters are: 1) Reynolds number, 2) Prandtl number, 3) temperature difference between fluid and cylinder and 4) conductivity ratio. The latter is given by

$$\Lambda = \frac{k_p}{k_f} = \frac{k_p}{D_{\text{thermal}} c_p \rho} = \frac{k_{pf}}{D_{\text{thermal}}}, \tag{27}$$

where $k_{pf} = k_p/(c_p\rho)$. Since we keep the thermal diffusivity of the fluid constant when changing the conductivity ratio, the conductivity ratio is essentially changed by changing k_{pf}.

Table 1
Range of parameters studied.

Parameter	Values
Reynolds number [-]	100, 400, 1600
Conductivity ratio [-]	1, 12, 144
ΔT [K]	0, 1, 3, 10, 173, 400

For each of the parameters listed in Table 1, the impaction efficiencies of particles in the Stokes number range between 0.01 and 10 are obtained from the DNS simulations.

For each particle size (Stokes number), a certain number of particles have to impact the surface to get sufficient statistics in order to estimate an accurate impaction efficiency. Since the impaction efficiency decreases significantly with Stokes number, we have to release more small than large particles. Therefore, 15,000 particles are released for each particle size for $\text{St} > 1$, 200,000-400,000 for particles with $0.1 < \text{St} < 1$, and 2 million for each particle size for particles with $\text{St} < 0.1$. The particles are inserted over several vortex shedding times to mitigate the effect the instantaneous vortex shedding could have on the results.

All simulations can be described by the $n = 10$ unique and independent variables that are listed in Table 2. From the table we see that all variables involve a total of $k = 4$ different units (m, s, kg and K).

From the Buckingham-Pi theorem, we thus know that the simulations can be described by exactly $p = n - k = 6$ different dimensionless numbers. These dimensionless numbers are listed in Table 3.

In this work, we study the effect of variations in all of these dimensionless numbers, except for S_ρ, which is always kept constant at $S_\rho = 1000$. Changing S_ρ means that another dimensionless number, $D/d_p = \sqrt{\text{Re}S_\rho/(18\text{St})}$, will change. The effect of this is a shift in the level of the interception mode. I.e., a shift will occur in the mode by which very small particles intercept the cylinder when only pure impaction is accounted for. This is important to account for when comparing simulation results with different values of S_ρ, which for example is done in Fig. 11b of Kleinhans et al. [25]. The parameter variations in our simulations are listed in Table 4.

5. Results

In this section we will study the effect of the thermophoretic force on the impaction efficiency. In particular, we will look at how the impaction efficiency is affected by changes in the Reynolds number, temperature difference and conductivity ratio.

Table 2
Independent variables describing the simulations.

Variable	value	unit	Description
k_{pf}	(1.43, 17.2 or 206) $\times 10^{-3}$	m^2/s	Norm. therm. diff. of particles
ρ_p	400	kg/m^3	Material density of particles
d_p	varies	m	Diameter of particles
ρ	0.4 (at inlet)	kg/m^3	Material density of fluid
D_{thermal}	1.43×10^{-3}	m^2/s	Thermal diffusivity of fluid
u	1 (at inlet)	m/s	Velocity of fluid
ν	(6.25, 25 or 100)$\times 10^{-5}$	m^2/s	Viscosity of fluid
D	0.1	m	Diameter of cylinder
T_f	873	K	Far-field temperature of fluid
T_c	700–873	K	Temperature of cylinder

Table 3
Dimensionless numbers describing the simulations.

Dimensionless number	Description
$\Lambda = k_{pf}/D_{\text{thermal}}$	Conductivity ratio
$\text{Re} = Du/\nu$	Reynolds number
$\Theta = T_f/T_c$	Temperature ratio between far-field and cylinder
$S_\rho = \rho_p/\rho$	Density ratio between particle and fluid
$\text{St} = S_\rho d_p^2 u/(18\nu D)$	Stokes number
$\text{Pr} = \nu/D_{\text{thermal}}$	Prandtl number

Table 4
Overview of the simulated cases. Particles with Stokes number ranging from 0.01 to 10 are inserted in all cases.

Sim.	Re	Pr	ΔT	Λ
'Base case'	100	0.7	-	-
0	100	0.7	173	12
C1	100	0.7	173	1
C144	100	0.7	173	144
dT3	100	0.7	3	12
dT10	100	0.7	10	12
dT400	100	0.7	400	12
R400	400	0.7	173	12
R1600	1600	0.7	173	12
RPv400	400	0.175	173	12
RPv1600	1600	0.043	173	12

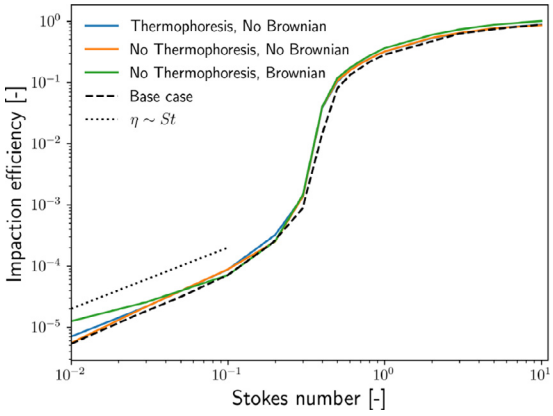

Fig. 4. Comparison of η for data from Aarnes et al. [5] with data obtained from an isothermal case with and without thermophoretic force.

Aarnes et al. [5] used DNS to find the efficiency by which particles embedded in an isothermal cross flow impact on a cylinder. In their study they used an overset grid, but they did not consider the thermophoretic force nor did they solve the energy equation. In the following, we will use their results as a reference case, from now on called the "Base case". Fig. 4 compares the impaction efficiency of the "Base case" with what is found for the same conditions in the current work. From the figure, we see that the impaction efficiency shows a slight decrease with decreasing Stokes number for Stokes numbers above 1, followed by a steep drop of impaction efficiency in the Stokes number range between 0.1 and 1. For even smaller Stokes numbers, the impaction efficiency decreases linearly with decreasing Stokes number. As expected, our simulations of isothermal cases both with (blue line) and without (orange line) the thermophoretic force (Eq. (10)) included yield the same impaction efficiency profile as the 'Base case'. A case with Brownian forces on the particles has also been performed, and a weak effect of Brownian forces for the smallest Stokes numbers is visible. This effect is quite weak, and, as we shall see, the thermophoretic force will have a much stronger effect on the impaction efficiency even for very small temperature gradients.

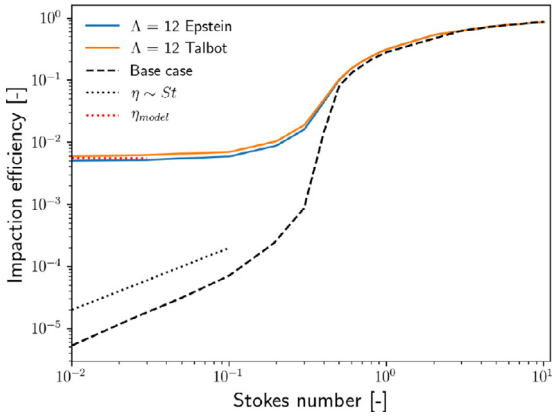

Fig. 5. Front side impaction efficiency as a function of Stokes number. For the non-isothermal cases ($\Delta T = 173$ K), results with thermophoretic factors as given by Epstein and Talbot are compared. The red dotted line corresponds to the impaction efficiency predicted by the model for small Stokes numbers as given in Eq. (25). (For interpretation of the references to colour in this figure legend, the reader is referred to the web version of this article.)

In Fig. 5, the "Base case" (isothermal) is compared to non-isothermal cases with thermophoresis. Simulations with a temperature difference between the inlet gas and the cylinder surface of $\Delta T = 173$ K and a particle conductivity ratio of 12 was used for the thermophoretic cases. It was shown in § 2.2 that the models of Epstein and Talbot gave comparable values of Φ. The two solid lines in Fig. 5 show the corresponding difference in impaction efficiency. For the smaller particles, the impaction efficiency predicted by the model of Talbot et al. is only about 10% higher than the one predicted by Epstein, a difference that disappears for larger particles. It is clear from our results that the particle impaction is unaffected by the thermophoretic force for large Stokes numbers, while it is dominated by the thermophoretic force for small Stokes numbers. In stark contrast to what is observed for the isothermal case, the impaction efficiency becomes independent of the particle size for small particles. The theoretical prediction of the impaction efficiency for small Stokes numbers, as presented in Eq. (25), is repre-

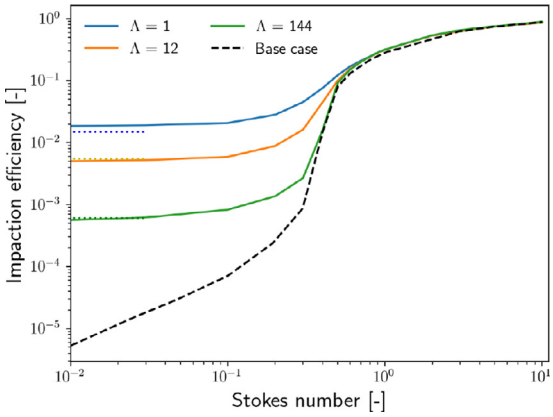

Fig. 6. Front side impaction efficiency over Stokes number for different conductivity ratios. This corresponds to simulations 'Base case', 0, C1 and C144 as listed in Table 4. The dotted lines correspond to the impaction efficiency predicted by Eq. (25) for small Stokes numbers.

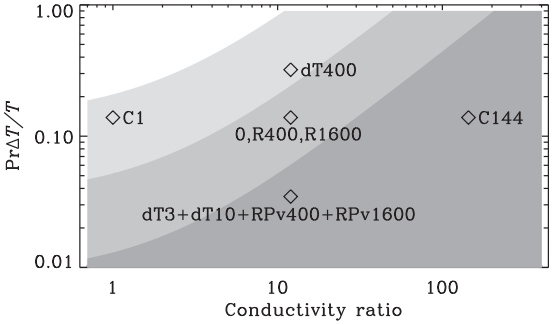

Fig. 7. For the simulations marked in the grey area, the model from Eq. (25) is applicable. From lightest to darkest the grey areas correspond to $\alpha = 1.0$, 0.5 and 0.25. For the cases that are in the white area, however, Eq. (26) yields no applicability. The simulations with different Reynolds number and constant Prandtl number ("R400" and "R1600") are positioned at the same place as simulation "0".

sented by the red dotted horizontal line in the figure and one can see that it fits well with the numerical results for St < 0.1.

The effect of different conductivity ratios on the impaction efficiency is shown in Fig. 6. We see that the impaction efficiency for small Stokes numbers is higher for lower values of the conductivity ratio. This is because a small conductivity ratio yields a large thermophoretic force term (Φ), which results in a large thermophoretic force, leading to high impaction efficiency. This effect can also be seen directly from Eq. (25), where the impaction efficiency for small Stokes numbers scales linearly with Φ. When the simplified expression for Φ is used, a linear dependence on Φ means that the impaction efficiency is inversely proportional with $(2 + \Lambda)$.

The applicability of our model, which is given as a function of α in Eq. (26), is visualised in Fig. 7 for different values of α. From these results it is apparent that the model is not strictly applicable for the smallest conductivity ratio (case C1) if $\alpha \lesssim 0.5$. This is probably the reason why the modelled impaction efficiency at small Stokes numbers for $\Lambda = 1$ (as represented by the horizontal blue dotted line in Fig. 6) deviates somewhat from the simulated results (blue solid line). It should be noted that a conductivity ratio of 1 is quite improbable. Zhang et al. [26] give a value for the conductivity ratio of small char particles of $\Lambda \approx 9$. The conductivity ratio may, however, be different for other solids. In the following we use $\Lambda = 12$ as a baseline for our simulations.

By comparing how well our model reproduces the simulation results, it seems reasonable to assume that $\alpha \sim 0.5 - 1.0$. Based on Eq. (26), we can then find that for char particles ($\Lambda \approx 10$), the more stringent value of α (=0.5) results in the model being applicable as long as ΔT is less than $\approx 30\%$ of the far field temperature for fluids with Pr = 0.7. For the same conditions and $\alpha = 1.0$, our model is applicable for all values of ΔT.

In the left hand panel of Fig. 8, the impaction efficiency is shown as a function of angular position for different Stokes numbers for simulations with a conductivity ratio of $\Lambda = 12$. (The centre-line is at 270 degrees.) For the largest Stokes number (St = 0.9), all impaction occurs within an angle, $\theta_{\max}$, that is smaller than 60 degrees from the centre line. This is consistent with the findings of Haugen and Kragset [3] without thermophoresis. When thermophoresis is accounted for, however, the particles with smaller Stokes numbers impact the entire frontal surface of the cylinder. By increasing the strength of the thermophoretic force, which is here done by decreasing the conductivity ratio to unity, we see from the right hand panel of Fig. 8 that the angular position of impaction becomes almost uniform for the smaller particles.

Since the gas is an ideal gas, the cylinder is surrounded by a boundary layer of densified gas with a significant temperature gradient for cases with large temperature differences. A larger temperature difference yields a stronger thermophoretic force, which again results in a higher impaction efficiency for small particles. As can be seen from Fig. 9, the results computed from our mathematical model (dotted lines) fit the simulation results (solid lines) well for all temperature differences studied here (3 K < ΔT < 400 K). Yet we see from Fig. 7 that $\Delta T = 400$ K is close to the limit of the applicability of the mathematical model, so caution is advised when using the model in this upper temperature range.

Lastly we investigate the effect of Reynolds number on the impaction efficiency. In this work, we increase the Reynolds number by decreasing the viscosity. While doing this, we also increase the resolution in order to properly resolve the boundary layer, which

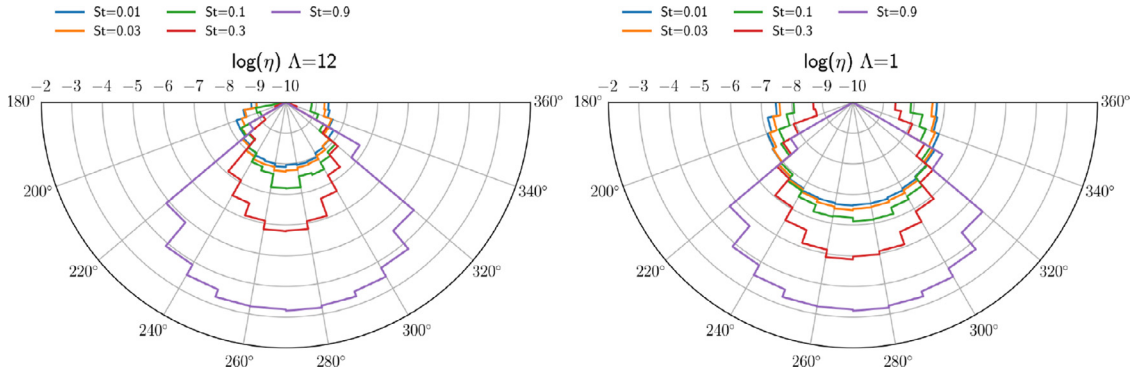

Fig. 8. Front side impaction angle for Λ=12 (left panel) and Λ=1 (right panel). Simulations 0 and C1, respectively.

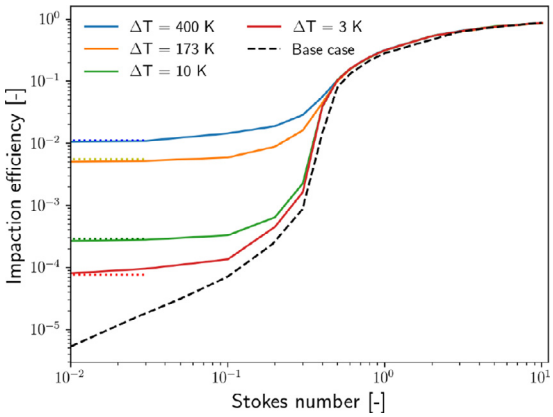

Fig. 9. Impaction efficiency over Stokes number for different cylinder temperatures (simulations 0, dT3, dT10 and dT400 as listed in Table 4). A high temperature difference increases η for small particles. The dotted lines correspond to the impaction efficiency predicted by Eq. (25) for small Stokes numbers.

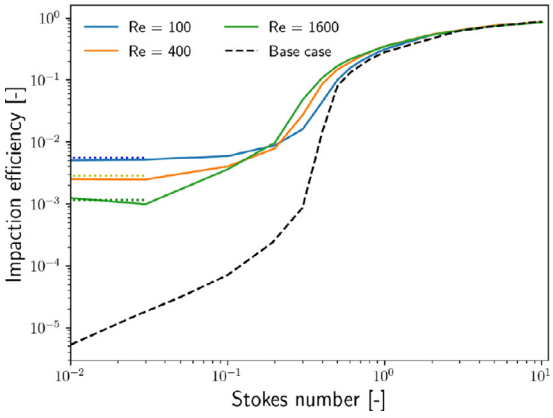

Fig. 10. Front side impaction efficiency over Stokes number for different flow Reynolds numbers. Simulations "0", "R400" and "R1600". Higher Reynolds numbers result in higher η for medium Stokes numbers, while for low Stokes numbers η is decreased. The dotted lines correspond to the impaction efficiency predicted by Eq. (25) for small Stokes numbers.

is thinner for higher Reynolds numbers. If the thermal diffusivity is changed linearly with viscosity, the Prandtl number is kept constant. This is what is done in Fig. 10, from which we see that increasing the flow Reynolds number results in higher front side impaction efficiencies for intermediate Stokes numbers in the range $0.2 < \mathrm{St} < 1$. This is qualitatively consistent with the findings of Haugen and Kragset [3] obtained for isothermal cases. From the results in Fig. 10 we also see that there is a clear but not dramatic Reynolds number effect for small Stokes numbers. This is supported by the model in Eq. (25), where the impaction efficiency for small Stokes numbers is inversely proportional to the square root of the Reynolds number. The prediction of Eq. (25) is represented by the horizontal dotted lines in Fig. 10, accurately reproducing the DNS results. We would also like to point out that, since higher Reynolds numbers are obtained by decreasing the viscosity, the particles for low Stokes numbers become quite small for cases with large Reynolds numbers. Unlike for isothermal cases, particle size does not, however, play any significant role in the impaction of particles with small Stokes number when the impaction mechanism is dominated by the thermophoretic force.

If the thermal conductivity of the fluid is not changed when changing viscosity, the Prandtl number is decreased for increasing Reynolds numbers, which is the case for the simulations shown in Fig. 11. Here we see that the Reynolds number dependence on the difference in impaction efficiency for the smaller Stokes numbers is larger than for the case with constant Prandtl number. This is also in agreement with Eq. (25) where lower Prandtl numbers yield lower impaction efficiencies, such that both the Prandtl and Reynolds number effects work in the same direction. By comparing the solid and the dotted lines, we see that the DNS results (solid lines) follows the model predictions (dotted lines) nicely.

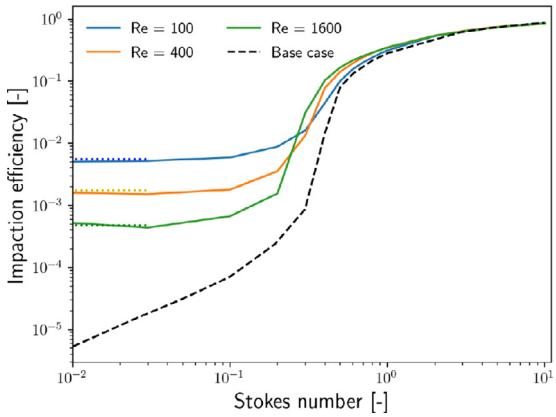

Fig. 11. Front side impaction efficiency over Stokes number for different flow Reynolds numbers. The Prandtl number is inversely proportional to the Reynolds number, such that it equals 0.7, 0.175 and 0.043 for Re =100, 400 and 1600, respectively. Simulations "0", "RPv400" and "RPv1600". Higher Reynolds numbers result in higher η for medium Stokes numbers, while for low Stokes numbers η is decreased. The dotted lines correspond to the impaction efficiency predicted by Eq. (25) for small Stokes numbers.

6. Conclusions

Using high order DNS, the effect of thermophoresis on the impaction efficiency of particles on a cylinder is studied for different values of the Reynolds number, conductivity ratio, temperature difference and particle Stokes number. It is found that the thermophoretic force has an insignificant effect on particles with Stokes numbers larger than ~ 0.5, but is often dominating the impaction rate for $\mathrm{St} \lesssim 0.3$. For small particles ($\mathrm{St} \lesssim 0.2$) we know that the impaction efficiency scales linearly with the Stokes number for isothermal cases. This is, however, not the case when impaction is controlled by the thermophoretic force. For such cases the impaction efficiency is independent of Stokes number for $\mathrm{St} \lesssim 0.1$. Furthermore, the impaction efficiency is larger for low conductivity ratios, high temperature differences and low Reynolds numbers.

An algebraic model (see Eq. (25)) that predicts the impaction efficiency due to thermophoresis has been developed based on fundamental principles. The validity of the model for a wide range of conditions has been verified against highly accurate DNS. The model can therefore be used for accurate analytical predictions of the impaction efficiency. The developed model is valid as long as the thermophoretic force is not very strong (see Eq. (26) and Fig. 7). Outside its range of validity, a reliable model does not yet exist. This should be the focus of future research.

Declaration of Competing Interest

The authors declare that they have no known competing financial interests or personal relationships that could have appeared to influence the work reported in this paper.

CRediT authorship contribution statement

Nils Erland L. Haugen: Conceptualization, Methodology, Software, Validation, Investigation, Resources, Data curation, Writing –

original draft, Writing – review & editing, Visualization, Supervision, Funding acquisition. **Jonas Krüger:** Software, Validation, Formal analysis, Investigation, Data curation, Writing – original draft, Visualization. **Jørgen R. Aarnes:** Conceptualization, Methodology, Software, Data curation, Writing – original draft, Writing – review & editing. **Ewa Karchniwy:** Software, Data curation, Writing – original draft, Writing – review & editing. **Adam Klimanek:** Resources, Writing – original draft, Writing – review & editing, Supervision, Funding acquisition.

Acknowledgements

This research was supported by The GrateCFD project [grant 267957/E20], which is funded by: LOGE AB, Statkraft Varme AS, EGE Oslo, Vattenfall AB, Hitachi Zosen Inova AG and Returkraft AS together with the Research Council of Norway through the ENERGIX program. Computational resources were provided by UNINETT Sigma2 AS [project numbers NN9405K]. We would also like to acknowledge that this research was partly funded by the Research Council of Norway (Norges Forskingsråd) under the FRINATEK Grant [grant number 231444] and by the grant "Bottlenecks for particle growth in turbulent aerosols" from the Knut and Alice Wallenberg Foundation, Dnr. KAW 2014.0048.

References

[1] U. Kleinhans, C. Wieland, F.J. Frandsen, H. Spliethoff, Ash formation and deposition in coal and biomass fired combustion systems: progress and challenges in the field of ash particle sticking and rebound behavior, Prog. Energy Combust. Sci. 68 (2018) 65–168, doi:10.1016/j.pecs.2018.02.001.

[2] R. Israel, D. Rosner, Use of a generalized stokes number to determine the aerodynamic capture efficiency to non-Stokesian particles from a compressible gas flow, Aerosol Sci. Technol. 2 (1982) 45–51.

[3] N.E.L. Haugen, S. Kragset, Particle impaction on a cylinder in a crossflow as function of stokes and Reynolds numbers, J. Fluid Mech. 661 (2010) 239–261, doi:10.1017/S0022112010002946.

[4] G. Kasper, S. Schollmeier, J. Meyer, J. Hoferer, The collection efficiency of a particle-loaded single filter fiber, J. Aerosol. Sci. 40 (2009) 993–1009, doi:10.1016/j.jaerosci.2009.09.005.

[5] J. Aarnes, T. Jin, C. Mao, N. Haugen, K. Luo, H. Andersson, Treatment of solid object in the pencil code using and immersed boundary method and overset grids, Geophys. Astrophys. Fluid Dyn. 114 (2020) 35–57, doi:10.1080/03091929.2018.1492720.

[6] J.R. Aarnes, N.E. Haugen, H.I. Andersson, Inertial particle impaction on a cylinder in turbulent cross-flow at modest Reynolds numbers, Int. J. Multiphase Flow 111 (2019) 53–61, doi:10.1016/j.ijmultiphaseflow.2018.11.001.

[7] A. Beckmann, M. Mancini, R. Weber, S. Seebold, M. Müller, Measurements and CFD modeling of a pulverized coal flame with emphasis on ash deposition, Fuel 167 (2016) 168–179, doi:10.1016/j.fuel.2015.11.043.

[8] X. Yang, D. Ingham, L. Ma, H. Zhou, M. Pourkashanian, Understanding the ash deposition formation in Zhundong lignite combustion through dynamic CFD modelling analysis, Fuel 194 (2017) 533–543, doi:10.1016/j.fuel.2017.01.026.

[9] H. Zhou, P.A. Jensen, F.J. Frandsen, Dynamic mechanistic model of superheater deposit growth and shedding in a biomass fired grate boiler, Fuel 86 (10) (2007) 1519–1533, doi:10.1016/j.fuel.2006.10.026.

[10] U. Kleinhans, C. Wieland, S. Babat, H. Spliethoff, Large eddy simulation of a particle-laden flow around a cylinder: importance of thermal boundary layer effects for slagging and fouling, Fuel 241 (2019) 585–606, doi:10.1016/j.fuel.2018.12.056.

[11] M. García Prez, E. Vakkilainen, T. Hyppnen, Unsteady CFD analysis of kraft recovery boiler fly-ash trajectories, sticking efficiencies and deposition rates with a mechanistic particle rebound-stick model, Fuel 181 (2016) 408–420, doi:10.1016/j.fuel.2016.05.004.

[12] L. Schiller, Z. Naumann, A drag coefficient correlation, Z. Ver. Dtsch. Ing. 77 (1935) 318.

[13] J. Tyndall, On dust and disease, Proc. R. Inst. 6 (1870) 1–14.

[14] F. Zheng, Thermophoresis of spherical and non-spherical particles: a review of theories and experiments, Adv. Colloid Interface Sci. 97 (1–3) (2002) 255–278.

[15] J. Young, Thermophoresis of a spherical particle: reassessment, clarification and new analysis, Aerosol Sci. Technol. 45 (8) (2011) 927–948.

[16] P. Epstein, Zur theorie des radiometers, Zeitschrift für Physik 54 (1929) 537–563.

[17] F. Sharipov, Data on the velocity slip and temperature jump coefficients [gas mass, heat and momentum transfer], in: 5th International Conference on Thermal and Mechanical Simulation and Experiments in Microelectronics and Microsystems, 2004. EuroSimE 2004. Proceedings of the, 2004, pp. 243–249, doi:10.1109/ESIME.2004.1304046.

[18] L. Talbot, R.K. Cheng, R.W. Schefer, D.R. Willis, Thermophoresis of particles in a heated boundary layer, J. Fluid Mech. 101 (4) (1980) 737–758, doi:10.1017/S0022112080001905.

[19] H. Schlichting, Boundary-Layer Theory, McGraw-Hill, 1979.

[20] A. Brandenburg, W. Dobler, Hydromagnetic turbulence in computer simulations, Comput. Phys. Commun. 147 (1) (2002) 471–475.

[21] A. Brandenburg, A. Johansen, P.A. Bourdin, W. Dobler, W. Lyra, M. Rheinhardt, S. Bingert, N.E.L. Haugen, A. Mee, F. Gent, N. Babkovskaia, C.C. Yang, T. Heinemann, B. Dintrans, D. Mitra, S. Candelaresi, J. Warnecke, P.J. Kpyl, A. Schreiber, P. Chatterjee, M.J. Kpyl, X.Y. Li, J. Krger, J.R. Aarnes, G.R. Sarson, J.S. Oishi, J. Schober, R. Plasson, C. Sandin, E. Karchniwy, L.F.S. Rodrigues, A. Hubbard, G. Guerrero, A. Snodin, I.R. Losada, J. Pekkil, C. Qian, The pencil code, a modular MPI code for partial differential equations and particles: multipurpose and multiuser-maintained, J. Open Source Softw. 5 (2021) 2684, doi:10.21105/joss.02684.

[22] A. Brandenburg, The Pencil Code, 2018. URL (pencil-code.nordita.org), available from: https://github.com/pencil-code.

[23] T. Poinsot, S. Lele, Boundary conditions for direct simulations of compressible viscous flows, J. Comput. Phys. 101 (1) (1992) 104–129.

[24] J. Aarnes, N. Haugen, H. Andersson, High-order overset grid method for detecting particle impaction on a cylinder in a cross flow, Int. J. Comput. Fluid Dyn. 33 (2019) 43–58.

[25] U. Kleinhans, C. Wieland, S. Babat, G. Scheffknecht, H. Spliethoff, Ash particle sticking and rebound behavior: amechanistic explanation and modeling approach, Proc. Combust. Inst. 36 (2) (2017) 2341–2350, doi:10.1016/j.proci.2016.05.015.

[26] X. Zhang, A. Dukhan, I. Kantorovich, E. Bar-Ziv, The thermal conductivity and porous structure of char particles, Combust. Flame 113 (4) (1998) 519–531, doi:10.1016/S0010-2180(97)00246-0.